

Crystallization of Self-Propelled Hard Discs

G. Briand and O. Dauchot

EC2M, UMR Gulliver 7083 CNRS, ESPCI ParisTech, PSL Research University, 10 rue Vauquelin, 75005 Paris, France

(Received 10 May 2016; published 24 August 2016)

We experimentally study the crystallization of a monolayer of vibrated discs with a built-in polar asymmetry, a model system of active liquids, and contrast it with that of vibrated isotropic discs. Increasing the packing fraction ϕ , the quasicontinuous crystallization reported for isotropic discs is replaced by a transition, or a crossover, towards a “self-melting” crystal. Starting from the liquid phase and increasing the packing fraction, clusters of dense hexagonal-ordered packed discs spontaneously form, melt, split, and merge, leading to a highly intermittent and heterogeneous dynamics. For a packing fraction larger than ϕ^* , a few large clusters span the system size. The cluster size distribution is monotonically decreasing for $\phi < \phi^*$, nonmonotonic for $\phi > \phi^*$, and is a power law at the transition. The system is, however, never dynamically arrested. The clusters permanently melt from place to place, forming droplets of an active liquid which rapidly propagate across the system. This self-melting crystalline state subsists up to the highest possible packing fraction, questioning the stability of the crystal for active discs unless it is at ordered close packing.

DOI: [10.1103/PhysRevLett.117.098004](https://doi.org/10.1103/PhysRevLett.117.098004)

Assemblies of self-propelled particles are prone to a number of novel collective behaviors specific to these intrinsically out-of-equilibrium systems [1,2]. As such, they open new paths for designing smart materials, but also challenge our fundamental understanding of out-of-equilibrium matter.

On one hand, the crystallization [3,4] and the glass transition [5,6] of mechanically agitated grains, beads, or discs conserve the essential properties of their equilibrium counterparts. Even in the case of significantly inelastic collisions, when the 2D crystallization turns into a first-order transition with phase coexistence [7], it retains an equilibrium flavor. A similar result is obtained in a model of repulsive active Brownian particles (ABPs) [8]. However, on the other hand, there are indications that the dense phases of active matter cannot so easily be mapped onto equilibrium situations. The transition shift to higher densities [8–14] cannot be explained by a simple scaling argument using effective temperature. Active glasses exhibit very peculiar structural heterogeneity [11]. Their dynamics is slower at short times, but faster at large times; this suggests that the system is effectively “cooler” than its equilibrium counterpart but also that it accesses relaxation pathways, which are closed at equilibrium [12,13]. These observations point at a strong decoupling between structure and dynamics, as also underlined in [14]. Whether a simple yet real system of active particles crystallizes following an equilibrium scenario remains an open question of both fundamental and practical interest.

In this Letter we take advantage of a 2D experimental system of self-propelled polar discs [15,16], for which high packing fractions ϕ can be reached, to perform the first experimental study of crystallization in a system of self-propelled discs. We identify a radically new scenario,

which shares no resemblance with the quasicontinuous, equilibriumlike crystallization observed for isotropic discs or with a first-order-like equilibrium phase coexistence. Starting from the liquid phase and increasing the packing fraction, clusters of dense hexagonally ordered packed discs spontaneously form, melt, split, and merge, leading to a highly intermittent and heterogeneous dynamics Fig. 1. At $\phi = \phi^*$, the largest clusters percolate. The system is, however, never dynamically arrested. Local excitations form and propagate across the system, permanently melting the putative crystalline phase.

The experimental system is made of vibrated discs with a built-in polar asymmetry, which enables them to move coherently, and has been described in detail previously

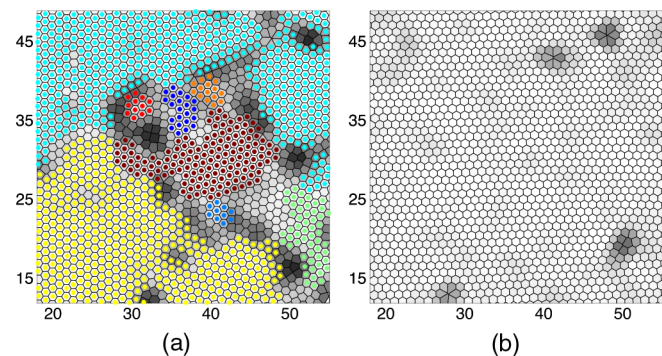


FIG. 1. Crystallization of a vibrated monolayer of (a) polar and (b) isotropic discs. Packing fraction $\phi = 0.84$. The gray colormap indicates the local orientational order parameter ψ_6^l (see text for details). For the polar discs, distinct crystal clusters (in color) are present, while (apart from local defects) a homogeneous ordered phase is observed in the isotropic case. (See also the movies in Supplemental Material for the dynamics [23].)

[16]. The polar particles are micromachined copper-beryllium discs (diameter $d = 4$ mm) with an off-center tip and a glued rubber skate located at diametrically opposite positions (total height $h = 2$ mm). These two “legs,” with different mechanical response, endow the particles with a polar axis. Under proper vibration, the discs perform a persistent random walk, the persistence length of which is set by the vibration parameters. We also use plain rotationally invariant discs (the same metal, diameter, and height), hereafter called the “isotropic” discs. Here we use a sinusoidal vibration of frequency $f = 95$ Hz and relative acceleration to gravity $\Gamma = 2\pi af^2/g = 2.4$. The motion of the particles is tracked using a standard CCD camera at a frame rate of 25 Hz. In the following, the unit of time is set to be the inverse frame rate and the unit length is the particle diameter. Within these units, the resolution on the position \vec{r} of the particles is better than 0.05; that on the orientation \vec{n} is of the order of 0.05 rad. In the present case, the vibration conditions are such that the persistence length of an isolated polar particle $\xi \approx 5$ is 2–3 times smaller than in [15]; no collective motion sets in and the system is closer to existing models, for which the dynamical rules guarantee self-propulsion without alignment [17]. In the following, particle trajectories are tracked within a circular region of interest (ROI) of diameter 50, where the long-time averaged density field is homogeneous. The average packing fractions ϕ measured inside the ROI range from 0.42 to 0.84, and the total number of particles typically from 1500 to 3000.

The nature of the liquid-solid transition for hard discs [18] has been a matter of intense debate until recently [19], when it was shown that the transition occurs with two steps as in the Kosterlitz-Thouless-Halperin-Nelson et Young scenario [20–22], but with the first transition between the liquid phase and the hexatic phase—with orientational but no translational order—being weakly discontinuous. Here also, the transition observed for the isotropic particles follows this quasicontinuous scenario, with an homogeneous increase of both $\rho(\mathbf{r})$ and $\psi_6(\mathbf{r})$, when the packing fraction $\phi > \phi^\dagger \approx 0.71$. We leave aside the detailed investigation of this now well-characterized transition to concentrate on the case of the polar particles.

The structure of the bidimensional packing is characterized using standard equilibrium tools. Starting from the particle positions at all times $\mathbf{r}_p(t)$, we compute the density field $\rho(\mathbf{r})$ and its fluctuations as characterized by the pair correlation function $g_2(r)$,

$$g_2(r) = \left\langle \frac{\sum_{p \neq q} \delta(r - |\mathbf{r}_q - \mathbf{r}_p|)}{2\pi N r} \right\rangle, \quad (1)$$

where N is the number of particles within the ROI at time t and $\langle \cdot \rangle$ denotes the time average. We also compute the instantaneous orientational order parameter ψ_6 at the particle scale, its fluctuations, and their correlations $g_6(r)$,

$$\psi_6^p = \left[\frac{1}{n_p} \sum_{\langle pq \rangle} \exp(6i\theta_{pq}) \right], \quad (2)$$

$$g_6(r) = \left\langle \frac{\sum_{p \neq q} \psi_6^p \psi_6^q \delta(r - |\mathbf{r}_q - \mathbf{r}_p|)}{2\pi N(N-1)r} \right\rangle, \quad (3)$$

where $\sum_{\langle pp' \rangle}$ denotes the sum over the n_p neighbors of particle p identified from a Voronoi tessellation, and $[\cdot]$ a coarse-graining of the field on the first neighbor’s shell.

Figure 2 synthesizes the structural properties of the polar disc system and how they compare with the case of the isotropic discs. The pair correlation function [Fig. 2(a)] clearly exhibits the signature of an emerging crystal structure for packing fractions similar to that of the polar

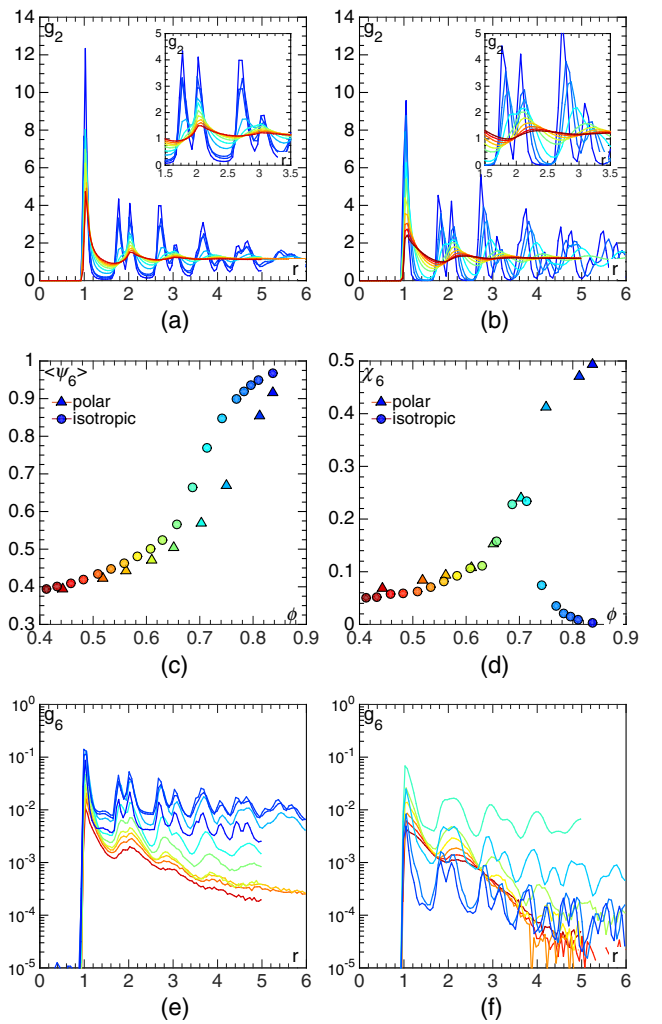


FIG. 2. Structural properties for $\phi \in [0.42 - 0.84]$ color coded from red to blue. Top: Pair correlation function for the (a) polar and (b) isotropic discs. Inset: zoom on second and third peaks. Middle: Dependence on ϕ of (c) the mean orientational order parameter $\langle \psi_6 \rangle$ and (d) its fluctuations. Bottom: Spatial correlation of ψ_6 for the (e) polar and (f) isotropic discs.

discs. However, a closer examination indicates that the locations of the secondary peaks coincide with those of the hexagonal close packing (HCP) as soon as they develop. Hence, the structures forming in the system of polar particles are densely packed hexagonally ordered clusters. This contrasts with the isotropic case [Fig. 2(b)], for which the peaks progressively shift to the right when further compressing the crystal, which is formed at ϕ^\dagger . Examining the statistics of $\psi_6 = (1/N)\sum_p \psi_6^p$, the orientational order parameter further confirms this observation [Figs. 2(c)–(d)]. In the case of the polar particles, the temporal average $\langle \psi_6 \rangle$ and temporal fluctuations, also called the susceptibility $\chi_6 = N\text{var}(\psi_6)$, smoothly increase with the packing fraction. There is no inflection in $\langle \psi_6 \rangle(\phi)$ and no maximum in $\chi_6(\phi)$, as observed in the case of the isotropic particles. This behavior reflects that for the polar discs the probability distribution function (PDF) of ψ_6 (not shown here) displays a bimodal shape, which is absent in the case of the isotropic discs. These observations all take root in the fact that the spatial correlation continuously grows, suggesting the existence of larger and larger domains; this is in contrast with the case of the isotropic discs, for which the spatial correlations of ψ_6 exhibit a nonmonotonic dependence on ϕ with a characteristic length scale that is maximal close to ϕ^\dagger [Figs. 2(e)–(f)].

The structural analysis reveals that the emergence of crystal order in the polar discs system follows a very different scenario from the one reported at equilibrium or for the isotropic discs. A coexistence picture, suggestive of a first-order transition, replaces that of a quasicontinuous transition. Turning to the study of the dynamics, we shall see, however, that no part of the system ever freezes; thus, this picture is not correct either.

The mean-square displacement (MSD) $\Delta^2(\tau) = \langle (1/N)\sum_p [\mathbf{r}_p(t+\tau) - \mathbf{r}_p(t)]^2 \rangle$ of the polar particles is superdiffusive until $\tau = 100$, where normal diffusion sets in, for all packing fractions [Fig. 3(a)]. This is in sharp contrast to the case of the isotropic discs [Fig. 3(b)], for which a clear plateau develops above ϕ^\dagger , associated with the trapping of the particles in the crystal structure. As a matter of fact, the short time dynamics of the polar particles does present a small sign of trapping at the largest ϕ , but this is rapidly wiped out by the longer-term superdiffusion. The decrease in magnitude of the MSD with increasing ϕ could suggest that larger and larger fractions of the particles are trapped, while the remaining ones behave as an active liquid. This is, however, not the correct picture, as demonstrated by the long-time behavior of the self-part of the dynamical overlap function $Q(a, \tau)$ and of the dynamical susceptibility $\chi_4(a, \tau)$ [24],

$$Q(a, \tau) = \left\langle \frac{1}{N} \sum_p \exp -\frac{[\mathbf{r}_p(t+\tau) - \mathbf{r}_p(t)]^2}{a^2} \right\rangle, \quad (4)$$

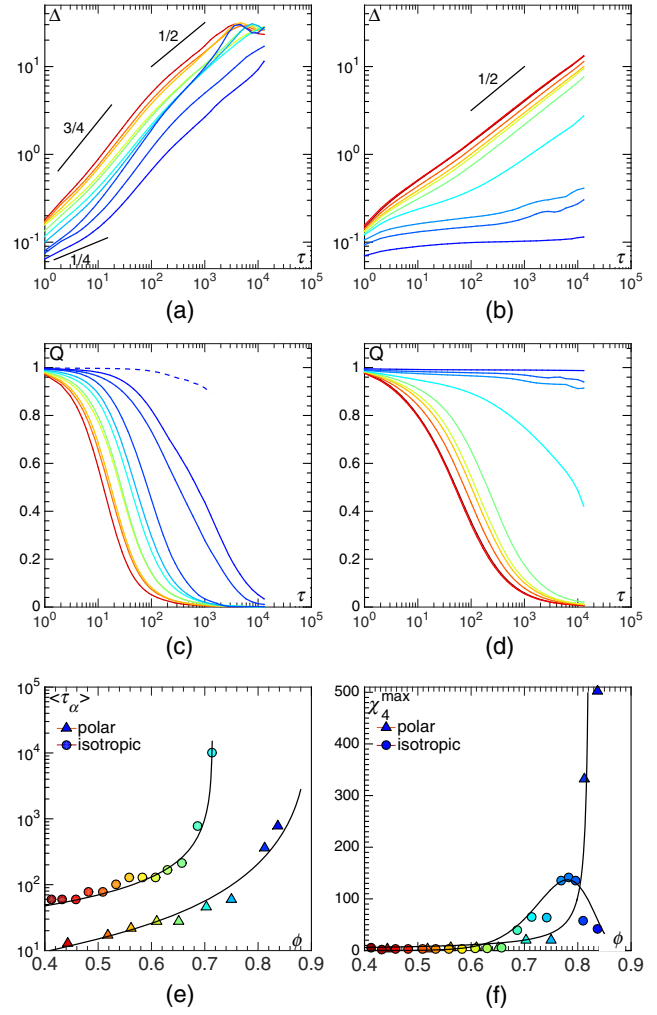


FIG. 3. Dynamical properties. Mean square displacement (top) and self-part of the dynamical overlap function (middle) for different ϕ for the [(a),(c)] polar and [(b),(d)] isotropic discs. The dotted line in (c) shows the relaxation of particles included in a crystalline cluster (see text for details). Bottom: (e) Relaxation time τ_α and (f) maximal dynamical susceptibility χ_4^{\max} as a function of ϕ . Same color code as in Fig. 2.

$$\chi_4(a, \tau) = N\text{var}\left(\frac{1}{N} \sum_p \exp -\frac{[\mathbf{r}_p(t+\tau) - \mathbf{r}_p(t)]^2}{a^2}\right), \quad (5)$$

which we evaluate for $a = 1$. Instead of developing a finite value plateau, $Q(\tau)$, pointing at a fraction of dynamically arrested particles, always rapidly decreases to zero. All particles move more than one diameter on time scales of the order of 5000 [Fig. 3(c)], and no part of the system is dynamically arrested. By comparison, in the case of the isotropic particles, $Q(\tau)$ clearly converges towards a plateau close to one [Fig. 3(d)] when $\phi > \phi^\dagger$. Accordingly, while the relaxation time τ_α , defined by $Q(\tau_\alpha) = 0.5$, diverges sharply at ϕ^\dagger pointing at the crystallization transition for the isotropic particles, it mildly increases

for the polar ones [Fig. 3(e)]. Conversely, the maximum of the dynamical susceptibility, $\chi_4^{\max} = \max[\chi_4(\tau)]$, which takes place for $\tau \approx \tau_\alpha$ and quantifies the heterogeneities of the dynamics, exhibits a mild maximum in the transitional regime for the isotropic particles, while it becomes increasingly large when entering the coexistence regime for the polar particles [Fig. 3(f)]. For the isotropic particles, the dynamical heterogeneities reflects the structural ones: they gently increase in the transitional regime and vanish in the homogeneous crystalline phase. The case of the polar particles is more intriguing: not only do the dynamical heterogeneities increase continuously with the packing fraction, they also increase much faster than the relaxation time, pointing at a peculiar collective behavior at some intermediate packing fraction $\phi^* \approx 0.82$.

Further insight into this unexpected feature comes from a closer inspection of the densely ordered clusters unveiled by the structural analysis (see also the movies in the Supplemental Material [23]). A cluster is defined as a group of particles sharing six neighbors “in contact” ($0.9d < r_{ij} < 1.1d$). By convention, the neighbors are also included in the cluster. The number of clusters [Fig. 4(a)] fluctuates around a steady value, with no sign of coarsening, at all packing fractions. The average number of clusters is at a maximum for $\phi \approx \phi^*$. For $\phi < \phi^*$, clusters split and merge, leading to a steady distribution of cluster sizes $p(s)$ decreasing exponentially [see Fig. 4(b)]. As the packing fraction increases towards ϕ^* , the distribution approaches a power law $p(s) \sim s^{-\gamma}$, $\gamma = 2$, with a system size cutoff. For $\phi > \phi^*$ it is nonmonotonic, and a peak at large cluster sizes emerges. This behavior is reminiscent of a transition reported in several experiments with bacteria [25–27] and simulations [27,28]. Also, the value of $\gamma = 2$ is very close to the one obtained in simulations of self-propelled rods ($\gamma = 1.9$), in experiments on myxobacteria ($\gamma = 1.88$), and is compatible with that obtained from simplified kinetic models of cluster dynamics [29,30] [the cluster size distribution $p(s)$ is easily related to $\tilde{p}(s)$, the probability of a particle to be in a cluster of size s : $\tilde{p}(s) \propto sp(s)$].

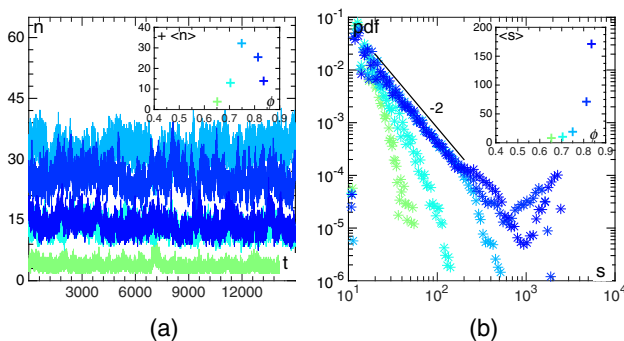


FIG. 4. HCP cluster statistics. (a) Steady evolution of the number of clusters (inset: average number of cluster vs ϕ) and (b) cluster size distributions (inset: average cluster size vs ϕ) for the five largest packing fractions where clusters appear.

We note that the present observation of a phase of dynamical clusters demonstrates that diffusiophoretic sensing is not necessary for this phase to take place. Even the largest clusters, which form for $\phi > \phi^*$ and span the system size, are never dynamically frozen: the locally ordered structure spontaneously melts (see also the movies in the Supplemental Material [23]), leading to the intermittent formation of active droplets rapidly propagating and relaxing the system.

The above scenario suggests that no crystal phase stabilizes below HCP. To confirm this observation, we compute the dynamical overlap function $Q(\tau)$ for a set of particles which remain at all times inside the longest-lived cluster, at the largest packing fraction $\phi = 0.837$ explored here. The advection of the cluster is removed by computing the particle displacements in the frame of their center of mass. Doing so, we evaluate the relaxation time, of the polar particles crystalline state. The result, displayed as the dashed line on Fig. 3(c), shows that (i) the relaxation is faster than that of the passive crystal at the same packing fraction, indicating internal relaxation processes much faster than equilibrium defects dynamics and (ii) we could not compute the relaxation on longer time scales because of the cluster splitting into pieces. Investigating in detail the local melting processes at play is beyond the scope of the present Letter. Visual inspection, however, allows us to propose two complementary mechanisms, the last one being admittedly purely speculative. First, the polar discs’ tendency to cluster at the highest-possible packing fraction frees some volume, where melting can take place. Second, active stresses could also locally shear and enforce local melting.

Discussion.—Some of the above conclusions might be related to the confinement and finite size of our experimental system. As discussed in [29], depending on the splitting and aggregation processes, the transition can be a genuine phase transition (which persists in the thermodynamic limit) or just a crossover. In the latter case, the packing fraction ϕ^* would increase with system size and hit the HCP limit, and the system would remain in the many-cluster phase at all ϕ .

We conclude by pointing out interesting differences with previous studies. The present scenario is very different from that reported for ABPs [8]. This is all the more surprising given the absence of hydrodynamic interactions and similar values for the bare persistence length and the Peclet number. The difference could thus be attributed either to (i) the potential softness or (ii) the fact that ABP dynamics for the polar vector is decoupled from that of the velocity, which is not the case for the present self-propelled discs [17]. As compared to the numerical studies [11,12], the dynamical decoupling reported here is extreme in the sense that dynamical arrest only occurs at close packing. Confirming this in the case of a bidisperse disordered system would imply the absence of glass transition and

finite time relaxation up to jamming. Finally, classical nucleation theory was recently extended to active systems to describe the aggregation process following the motility induced phase separation [31,32]. Our results suggest that alternative, radically different approaches might be necessary to deal with the very dense phases of active matter.

We thank Michael Schindler for helpful suggestions on the clustering algorithm and Ludovic Berthier and Fernando Peruani for valuable comments. G. B. Ph. D. Grant was funded by Ecole Doctorale ED PIF.

-
- [1] M. C. Marchetti, J.-F. Joanny, S. Ramaswamy, T. B. Liverpool, J. Prost, M. Rao, and R. A. Simha, *Rev. Mod. Phys.* **85**, 1143 (2013).
- [2] A. Zöttl and H. Stark, *J. Phys. Condens. Matter* **28**, 253001 (2016).
- [3] J. S. Olafsen and J. S. Urbach, *Phys. Rev. Lett.* **95**, 098002 (2005).
- [4] P. M. Reis, R. A. Ingale, and M. D. Shattuck, *Phys. Rev. Lett.* **96**, 258001 (2006).
- [5] A. R. Abate and D. J. Durian, *Phys. Rev. Lett.* **101**, 245701 (2008).
- [6] R. Candelier, A. Widmer-Cooper, J. K. Kummerfeld, O. Dauchot, G. Biroli, P. Harrowell, and D. R. Reichman, *Phys. Rev. Lett.* **105**, 135702 (2010).
- [7] Y. Komatsu and H. Tanaka, *Phys. Rev. X* **5**, 031025 (2015).
- [8] J. Bialké, T. Speck, and H. Löwen, *Phys. Rev. Lett.* **108**, 168301 (2012).
- [9] S. Henkes, Y. Fily, and M. C. Marchetti, *Phys. Rev. E* **84**, 040301(R) (2011).
- [10] Y. Fily, S. Henkes, and M. C. Marchetti, *Soft Matter* **10**, 2132 (2014).
- [11] R. Ni, M. A. C. Stuart, and M. Dijkstra, *Nat. Commun.* **4**, 1479 (2013).
- [12] L. Berthier, *Phys. Rev. Lett.* **112**, 220602 (2014).
- [13] L. Berthier and J. Kurchan, *Nat. Phys.* **9**, 310 (2013).
- [14] G. Szamel, *Phys. Rev. E* **93**, 012603 (2016).
- [15] J. Deseigne, O. Dauchot, and H. Chaté, *Phys. Rev. Lett.* **105**, 098001 (2010).
- [16] J. Deseigne, S. Léonard, O. Dauchot, and H. Chaté, *Soft Matter* **8**, 5629 (2012).
- [17] K.-D. N. T. Lam, M. Schindler, and O. Dauchot, *New J. Phys.* **17**, 113056 (2015).
- [18] B. J. Alder and T. E. Wainwright, *Phys. Rev.* **127**, 359 (1962).
- [19] E. P. Bernard and W. Krauth, *Phys. Rev. Lett.* **107**, 155704 (2011).
- [20] J. M. Kosterlitz and D. J. Thouless, *J. Phys. C* **6**, 1181 (1973).
- [21] B. I. Halperin and D. R. Nelson, *Phys. Rev. Lett.* **41**, 519 (1978).
- [22] K. J. Strandburg, *Rev. Mod. Phys.* **60**, 161 (1988).
- [23] See Supplemental Material at <http://link.aps.org/supplemental/10.1103/PhysRevLett.117.098004> for movies of the cluster dynamics and of the orientational order parameter field.
- [24] *Dynamical Heterogeneities in Glasses, Colloids, and Granular Media*, edited by W. van Saarloos, L. Cipelletti, J.-P. Bouchaud, G. Biroli, and L. Berthier, *International Series of Monographs on Physics* Vol. 150 (Oxford University Press, New York, 2011).
- [25] H. P. Zhang, A. Be'er, E. L. Florin, and H. L. Swinney, *Proc. Natl. Acad. Sci. U.S.A.* **107**, 13626 (2010).
- [26] X. Chen, X. Dong, A. Be'er, H. L. Swinney, and H. P. Zhang, *Phys. Rev. Lett.* **108**, 148101 (2012).
- [27] F. Peruani, J. Starruß, V. Jakovljevic, L. Søgaard-Andersen, A. Deutsch, and M. Bär, *Phys. Rev. Lett.* **108**, 098102 (2012).
- [28] Y. Yang, V. Marceau, and G. Gompper, *Phys. Rev. E* **82**, 031904 (2010).
- [29] F. Peruani and M. Bär, *New J. Phys.* **15**, 065009 (2013).
- [30] D. Levis and L. Berthier, *Phys. Rev. E* **89**, 062301 (2014).
- [31] D. Richard, H. Löwen, and T. Speck, *Soft Matter* **12**, 5257 (2016).
- [32] G. S. Redner, C. G. Wagner, A. Baskaran, and M. F. Hagan, arXiv:1603.01362.